Spurt in the extrusion of polymeric melts : discrete models for relaxation oscillations

Please check the document version of this publication:

EINDHOVEN UNIVERSITY OF TECHNOLOGY
Department of Mathematics and Computing Science

RANA 98-20
November 1998

Spurt in the extrusion of polymeric melts; discrete
models for relaxation oscillations

by

A.A.F. van de Ven

Spurt in the extrusion of polymeric melts; discrete models for relaxation oscillations

Ven, A.A.F. van de
Eindhoven University of Technology,
Eindhoven, The Netherlands

Abstract. In the extrusion of polymer melts, several types of flow instabilities can occur. An example of this is spurt. Spurt is manifested by periodic oscillations in the pressure and the volumetric flow rate. These oscillations are of relaxation type. An extrusion through a cylindrical die is considered. A discrete model to describe spurt or relaxation oscillations is constructed. This model is based on observations from 3-dimensional theory. When spurt occurs, the shear rates very near to the wall of the die (i.e. in the spurt layer), are much higher than those in the kernel of the extruded polymeric melt. Therefore, the viscosity in the spurt layer is taken much smaller than in the kernel. In both regions a linear Newtonian fluid model is employed. A no-slip boundary condition at the wall is maintained. The model developed here, is compared to an analogous model, allowing for slip at the wall of the die. It is shown that corresponding results can be obtained from both models. Application of the model to a piston-driven extrusion flow shows the occurrence of spurt oscillations for a restricted range of prescribed inlet flow rates. The found oscillations are qualitatively in correspondence with experimental results.

1 Introduction

The manufacturing of plastic products from polymer melts is an industrial branch of strongly increasing economic importance. Many large companies are occupied with these kind of production processes. Polymers are frequently used in industrial applications because of their excellent material and mechanical properties, and their range of applications is extremely wide (from daily products as plastic bags to very advanced applications in automotive and aerospace industry). Industrial manufacturing of plastic products from polymer melts can be performed by processes such as extrusion, injection moulding, film-blowing, spinning or cable-coating, the final products being plastic household goods, sheets, wires or fibres, coated cables, and many others. Increase of operational profits requires higher production rates, however, without distorting the quality of the final product. Qualitative requirements on the final product concern strength, homogeneity, transparency, visual aspects, etc. The, often, contradictory requirements mentioned above have inspired especially the rheological world, but also scientists from applied mathematical physics and continuum mechanics, to produce an immense amount of literature (see, for instance, journals as Journal of Non-Newtonian Fluid Mechanics, and Journal of Rheology). In this field of research both material aspects, such as constitutive behaviour of highly nonlinear

1

viscoelastic fluids, as well as description of flow patterns (inclusive boundary conditions, e.g. slip or no-slip, and entrance and exit effects in dies or moulds) play a roll. In many of these investigations, stability comes into sight. Due to the nonlinearity of the problems concerned, mostly only numerical methods can lead to quantitative results, but nevertheless also several analytical approaches have been published. It is of trivial essence that all the results obtained should ultimately be compared with, or rather supported by, experimental data, which are extensively reported in literature.

In an extrusion process, molten polymer is pressed through a die, which can be cylindrical, plane, or annular. In injection moulding, molten polymer is pressed through a die into a mould, having the shape of the desired product (e.g. cups, spoons, or complete dashboards for cars). In fibre spinning, molten polymer is pressed through a small hole and stretched to a fibre. Finally, in cable-coating, molten polymer is extruded from an annular die on a solid (e.g. copper) wire travelling at high speed, thus covering the wire with a thin shield of polymer (e.g. for electric insulation).

In all the processes described above, distortions can show up when raising the production rate. These distortion always show up at the surface of the final product. Besides the smoothness of the surface, they also diminish qualitative requirements regarding strength and transparency. Therefore, these distortions are highly unwished-for, and should be avoided at all price. It is an important subject of research to find the origins of these distortions, and to discover how to improve the polymer and/or the geometry of the process in order to get rid of the distortions.

In this case-problem we concentrate on the extrusion of polymeric melts through a cylindrical capillary. The industrial aim of the process is to produce at an as high as possible rate great lengths of smooth plastic wires. However, when the production rate is increased above a certain critical level, distortions show up at the surface of the wire, making the final product worthless. These distortion are catched under the general name *extrusion instabilities*. The distortions can be of several types, having names as *sharkskin* (small periodic surface distortions), *spurt* (larger periodic surface and volume distortions), or *gross-melt fracture* (a complete non-periodic global distortion). As is shown in Figure 1 all of these types have their own specific regime of flow rates. In Figure 1 a typical flow curve (i.e. the stationary pressure in the extrusion barrel as function of the stationary flow rate through the die) for an extrusion process is drawn. Four regimes are distinguished in this figure:

- Regime I: the flow is regular here, yielding a smooth extrudate.

- Regime II: this is the sharkskin regime; small periodic disturbances show up at the surface of the layer.

- Regime III: spurt regime, showing alternate smooth and disturbed extrudate.

- Regime IV: gross melt fracture, a strongly distorted spiral-shaped extrudate.

Here, we restrict ourselves to spurt type instabilities. When an extrusion process is in the spurt regime, the extrudate shows alternating smooth and distorted regions. In this
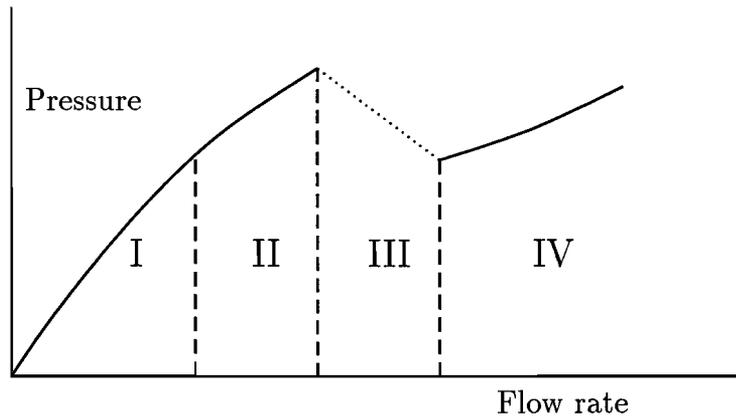
Figure 1: Stationary flow curve with (in)stability regimes

regime, the volumetric flow rate Q periodically jumps between a lower value ($\Rightarrow$ *smooth surface: classical flow*) and a much higher value ($\Rightarrow$ *distorted surface: spurt flow*). Also the pressure, driving the capillary flow, shows oscillations. These oscillations are many times observed in experiments, and look like relaxation oscillations (cf. [1]). Therefore, we shall refer to them as *spurt* or *relaxation oscillations*.

In spurt, as it is to be understood here, the flow profile looks strongly different in two regions:

- in the inner region (the kernel) the velocity gradient is small and the flow profile is flat, looking very much like cork flow; in this inner region the flow is similar to classical Poiseuille flow;

- in a very small region close to the wall the velocity profile is very steep, yielding very large values for the velocity gradient, or shear rate; this region is called the *spurt zone.*

In literature, spurt flow is explained in basically two different ways:

- as due to slip at the wall of the capillary; in this explanation, the spurt zone is in fact reduced to a surface layer in which slip takes place; the velocity at the wall is then no longer zero ([2], [3], and many others);

- as due to non-monotone constitutive behaviour ([4], [5], [6]).

Here, we shall adhere to the latter explanation in which spurt is called a *constitutive instability*, and in which the no-slip boundary condition is maintained.

Figure 2: Capillary rheometer

2   Extrusion model

The extrusion device we consider here is modelled as a capillary rheometer, consisting of a huge barrel filled with polymeric melt, closed at one side by a movable plunger, and on the other side connected to a narrow capillary (see Figure 2). The plunger moves with velocity V_0 and has an area A, whereas t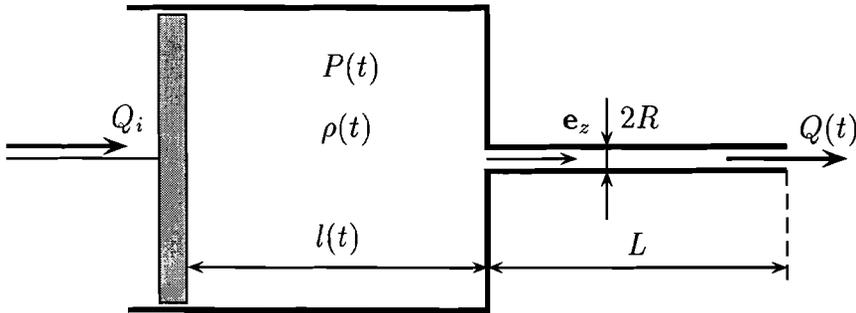he barrel has length l ($l = l(t) = l_0 - Vt$). Due to the plunger movement a pressure P is built up inside the barrel, and the melt is forced to leave the barrel and to flow into the capillary, with volumetric flow rate Q. At the end of the capillary, the melt leaves the capillary and the extrudate is formed. Since the flow in the barrel and in the capillary are of essentially different types, the two flows are also modelled in different ways. In the main part of the barrel the flow is an almost uniform compression flow ('plug flow'). The pressure becomes very high here due to the narrow inlet of the capillary, but the velocity is rather low because the barrel is very wide (as compared to the capillary). Hence, in the barrel the flow is compression dominated, and shear is negligible here. Thus, the compressibility of the melt inside the barrel must be taken into account, and the melt density ρ is variable. Since the flow in the barrel is uniform, P and ρ are only time-dependent, i.e. $P = P(t)$ and $\rho = \rho(t)$. On the other hand, the flow in the capillary is strongly shear dominated, due to the no-slip condition, which is assumed at the wall, and the relatively high velocity compared to that in the barrel. Then, the influence of compressibility is small, and the melt flowing through the capillary may be assumed incompressible. Hence, the melt flows through the whole capillary with uniform volumetric flow rate $Q = Q(t)$.

We first model the flow inside the barrel. The unknowns here are the density $\rho(t)$, the pressure $P(t)$ and the volumetric flow rate $Q(t)$ flowing from the barrel into the capillary. The relations to be used are:

- a global balance law for the total melt in the barrel:

$$\frac{d}{dt}(\rho A l) = -\rho A V_0 + \dot{\rho} A l = -\rho Q \ ,$$

4

where it is used that $\dot{l} = -V_0$;

- a constitutive (linearly elastic) compressibility law, relating the pressure to the density:

$$\frac{1}{\rho}\frac{d\rho}{dt} = \frac{1}{K}\frac{dP}{dt} ,$$

where K is the compression or bulk modulus of the polymer melt.

From these two laws the following relation between Q and P can be derived

$$\frac{dP(t)}{dt} = -\frac{1}{\chi}(Q(t) - Q_i) . \tag{1}$$

Here, $Q_i = AV_0$, the rate of volume displaced by the plunger, and $\chi = Al/K$: a material coefficient related to the compressibility.

For the shear dominated flow in the capillary (length L, radius R, $\pi R^2 \ll A$) we assume (r and z are cylindrical coordinates defined in the capillary):

- laminar incompressible flow:

$$\mathbf{v} = v(r,t)\mathbf{e}_z ;$$

- pressure linear in z, and equal to $P(t)$ at the inlet ($z = 0$) and zero at the outlet ($z = L$) of the capillary; this yields

$$\frac{\partial p}{\partial z} = -\frac{P(t)}{L} ;$$

- body force and inertia term are negligible ($\rho\dot{v} \approx 0$) in the equation of motion; this reduces this equation to its stationary version:

$$\nabla.\mathcal{T} = 0 ;$$

- constitutive equation for the stress of the (general) form

$$\mathcal{T} = -p\mathcal{I} + 2\eta_s\mathcal{D} + \mathcal{S}, \quad (\mathcal{D} = \frac{1}{2}(\nabla\mathbf{v} + (\nabla\mathbf{v})^T)),$$

where $2\eta_s\mathcal{D}$ represents a small Newtonian viscous component (which can be due to a small-molecule solvent, but just as well can represent the contribution due to a higher relaxation rate (cf. [5, Sect.2.6] or [9]), which becomes apparent for high shear rates), while $\mathcal{S}$ is the extra viscoelastic stress characterizing the polymer contribution. For moderate shear rates the viscoelastic stress $\mathcal{S}$ dominates the Newtonian term $2\eta_s\mathcal{D}$, but for higher shear rates (as occur in the spurt zone) the opposite is true.

5

With use of the four points listed above, it turns out that only the equation of motion in the axial z-direction is not trivially zero. This equation reads here

$$\frac{\partial T_{rz}}{\partial r} + \frac{T_{rz}}{r} = \frac{1}{r}\frac{\partial}{\partial r}(\eta w - S_{rz}) = \frac{\partial p}{\partial z} = -\frac{P(t)}{L} \ ,$$

where, $w = w(r,t) = -\partial v/\partial r$: the shear rate, and $S_{rz} = S_{rz}(r,t)$. After one integration with respect to r, where it is used that $(\partial v/\partial r)(0,t) = S_{rz}(0,t) = 0$, this equation can be evaluated to

$$\eta w(r,t) - S_{rz}(r,t) = \frac{P(t)}{2L}r \ , \tag{2}$$

The equations (1) and (2) must be supplemented by

- a constitutive equation for the extra shear stress S_{rz} (see Section 3) ;

- the no-slip boundary condition at the wall of the capillary $(r = R)$:

$$v(R,t) = 0 \ ; \tag{3}$$

- a relation for the volumetric flow $Q(t)$ reading

$$Q(t) = 2\pi \int_0^R rv(r,t)dr = \pi \int_0^R r^2 w(r,t)dr \ , \tag{4}$$

  where the latter result is derived after one integration by parts in which the no-slip boundary condition is used.

We proceed by making the basic equations (1) - (4) dimensionless. For the normalization of the shear stress, we use its initial viscosity η_0 and its first relaxation rate λ, both representative for small shear rates (see Section 3). That is, we take $S_{rz} = -\eta_0\lambda\hat{S}$, where $\hat{S}$ is the dimensionless shear stress. As we shall see in the next section, $\eta_0 \gg \eta_s$. The radial coordinate r is normalized on R ($\hat{r} = r/R$), the velocity on λR ($\hat{v} = v/\lambda R$), and the shear on λ ($\hat{w} = w/\lambda$). The dimensional flow rate and pressure are defined as

$$\hat{Q}_{(i)} = \frac{Q_{(i)}}{\pi\lambda R^3} \ , \qquad \hat{P} = \frac{R}{8\eta_0\lambda L}P \ ,$$

respectively. Finally, a time scale T, such that $\hat{t} = t/T$, is chosen as

$$T = \frac{8\eta_0\chi}{\pi}\frac{L}{R^4} \ ,$$

making the time derivative in (1) of $O(1)$. Note the dependence of T on the geometry of the die by the factor L/R^4. This factor is often encountered in experiments.

This normalization leads to the following set of equations (omitting the hats)

$$\frac{dP(t)}{dt} = Q_i - Q(t) \,, \tag{5}$$

$$\varepsilon w(r,t) + S(r,t) = 4P(t)r \,, \tag{6}$$

$$Q(t) = \int_0^1 r^2 w(r,t)dr \,, \tag{7}$$

$$v(1,t) = 0 \,. \tag{8}$$

In (6), $\varepsilon = \eta_s/\eta_0 \ll 1$, is a small parameter, relating the (very small) viscosity at high shear rates to the viscosity at moderate shear rates.

3 Constitutive model for the shear stress

In [4], [5], and [6], several constitutive models (JSO, KBKZ, with one or more relaxation rates) are studied, all having one common feature, knowing a non-monotone stationary shear curve (total stationary shear stress versus shear rate). An example of such a shear curve is drawn in Figure 3. The, for our considerations, most important consequence of this non-monotony is that the apparent viscosity for very high shear rates, as they occur in the spurt zone, is much smaller than the viscosity for the moderate shear rates in the kernel.

To visualize this, we consider a stationary solution of the system described in the preceding section. Let $\omega(r) = \lim_{t\to\infty} w(r,t)$ be the stationary value of the shear rate, and $F(r) = \lim_{t\to\infty}(4P(t)r)$, $r \in [0,1]$, the stationary value of the total shear stress. Then, as shown in [6, Sect.3], for small enough ε-values, the stationary shear curve is nonmonotone. This implies that for certain values of F the stationary solution of (6) is not unique. More relevant for our considerations is, however, the following observation: if $F(1)$ is large enough, there is a jump in $\omega(r)$ from a branch with rather low ω-values to a branch with much higher ω-values (see Figure 3). We refer to a stationary solution on the first branch as *classical flow*, and to one on the latter branch as *spurt flow*.

To distinguish between classical flow (moderate shear rates) and spurt flow (high shear rates) we propose the following (simplified) discrete model:

- In the classical flow zone we assume $\bar{S} = \omega$ and we neglect $\varepsilon\omega$ with respect to ω. In that case (6) reduces to (here $\bar{S}(r)$ and $\bar{P}$ are the stationary values of S and P)

$$\bar{S}(r) = \omega(r) = 4\bar{P}r \,. \tag{9}$$

This correspondences to Branch I in Figure 3.

- In the spurt zone, however, we neglect (motivated by the very low values of the viscosity at these high shear rates) $\bar{S}$ with respect to $\varepsilon\omega$, and then (6) yields

$$\varepsilon\omega(r) = 4\bar{P}r \,, \tag{10}$$
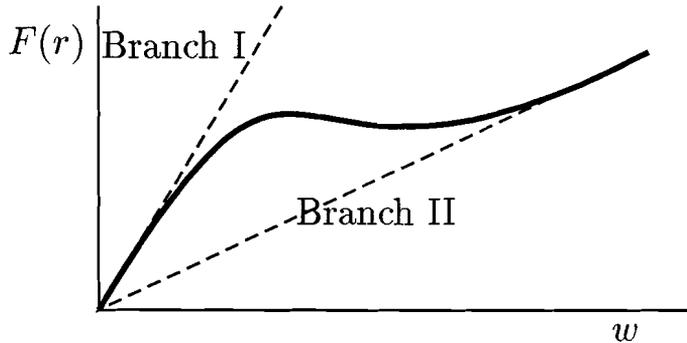
corresponding to Branch II.

Figure 3: A nonmonotone stationary shear curve

From the three-dimensional theories presented in [5] and [9], we mention the following results (which will form the basis for our discrete model to be presented in the next section):

1. For a certain range of prescribed inlet flow rates Q_i (piston-driven flow) spurt is found to occur. Spurt is manifested by a kink in the velocity profile ([5, Figure 2.2]): a narrow zone of very high shear rates is developed at the capillary wall. This results in a sudden increase in the outgoing flow rate $Q(t)$. This kinked velocity profile can be obtained by integration with respect to r of (9) and (10) (with $\omega(r) = -\partial v/\partial r$).

2. For a certain range of prescribed inlet flow rates Q_i periodic oscillations in both the pressure as well as the flow rate are found ([5, Figure 4.11]).

3. The transition from classical to spurt flow, and vice versa, is always very fast ([5, Figure 3.3]). During this fast transition the pressure remains (approximately) constant, whereas the flow rate suddenly jumps. The transition classical $\rightarrow$ spurt (loading trajectory) takes place at a higher pressure than the reverse transition spurt $\rightarrow$ classical (unloading trajectory) ([5, Sect.4.5]). This difference between loading and unloading explains *hysteresis*, a phenomenon that is observed in experiments by a.o. El Kissi and Piau [8]. A constitutive model in which loading and unloading trajects coincide, would theoretically exclude hysteresis.

4. During spurt the thickness of the spurt zone remains constant. This result is referred to as *shape memory* ([4] or [5, Sect.4.3 and 4.5]).

In the next section we construct on the basis of these observations from three-dimensional constitutive theories a simplified discrete model. This, mathematically simple, model will be able to predict relaxation oscillations in pressure and flow rate that are, at least qualitatively, similar to experimentally observed relaxation oscillations, reported in [7], [11] and [12].

4 Discrete model

The starting point for our discrete model is the possible existence of a spurt zone in capillary flow. During spurt, the spurt zone reaches from, say, $r = r^* < 1$, to $r = 1$, $(1 - r^* \ll 1)$, whereas in classical flow no spurt zone exists ($r^* = 1$). Hence, in accordance with (6), (9) and (10) we take

$$
\begin{aligned}
w(r,t) &= 4rP(t), && 0 \leq r < r^* \, ; \\
w(r,t) &= \frac{4rP(t)}{\varepsilon}, && r^* < r \leq 1.
\end{aligned}
\tag{11}
$$

With use of (11) in (7) the volumetric flow rate can be evaluated into

$$
\begin{aligned}
Q(t) &= \int_0^1 r^2 w(r,t)dr \\
&= P(t)\left((r^*)^4 + \frac{(1-(r^*)^4)}{\varepsilon}\right) \\
&\approx P(t)\left(1 + \frac{4}{\varepsilon}(1-r^*)\right),
\end{aligned}
\tag{12}
$$

since $(1 - r^*) \ll 1$. Assuming that $(1 - r^*) = O(\varepsilon)$, we define the normalized thickness of the spurt zone by

$$
R(t) = (1 - r^*)/\varepsilon \, .
\tag{13}
$$

Substitution of (13) into (12) yields

$$
Q(t) = (1 + 4R(t))P(t).
\tag{14}
$$

To make the model complete, we need an evolution equation for $R(t)$. This equation must match the four points listed in Section 3., especially the points 3. and 4. On the analogy of the slip model proposed by Greenberg and Demay in [2], which is also used in [7], we introduce the following evolution equation for the normalized thickness of the spurt zone,

$$
\frac{dR}{dt} = -\lambda[R(t) - \alpha H(P - B(Q))],
\tag{15}
$$

with λ and α material parameters, H the Heaviside function, and $B(Q)$ a switch curve, defined by

$$
B(Q) = \begin{cases}
Q_1, & Q < Q_1, \\[2mm]
Q_1 + \frac{Q-Q_1}{Q_2-Q_1}\left[\frac{Q_2}{1+4\alpha} - Q_1\right], & Q_1 < Q < Q_2, \\[2mm]
\frac{Q_2}{1+4\alpha}, & Q > Q_2,
\end{cases}
\tag{16}
$$

where Q_1 and Q_2 are two fixed values, such that $Q_2/(1 + 4\alpha) < Q_1 < Q_2$. This accounts for the fact that the transition spurt $\rightarrow$ classical takes place at a lower pressure than the

9
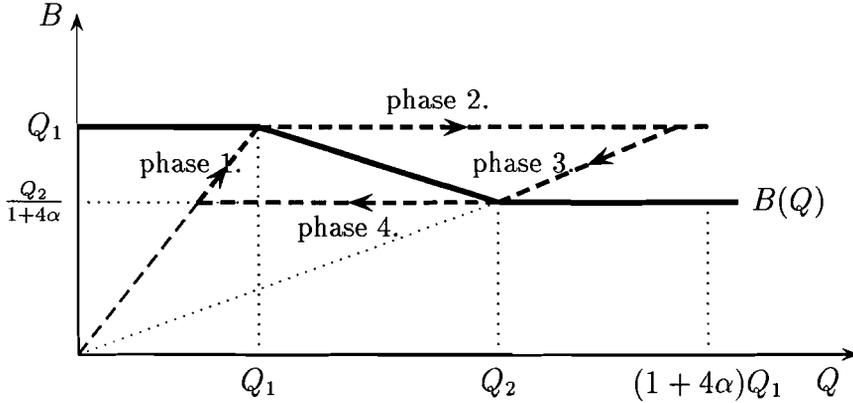
Figure 4: The switch curve $B(Q)$ (bold line). The dashed line represents the relaxation loop.

transition classical $\rightarrow$ spurt, in accordance with point 3., Section 3. It follows from (15) (see Section 6) that $R(t) = 0$ in classical flow, and that $R(t) = \alpha (= \text{constant})$ in spurt flow, in accordance with point 4.

The switch curve $B(Q)$ is depicted in Figure 4. Since, by assumption, the transition from classical to spurt flow, and vice versa, is very fast, we have $\lambda \gg 1$ in the normalized time scale used here.

Recapitulating, we have the following discrete model for the unknowns: $P(t), Q(t)$, and $R(t)$.

$$
\begin{aligned}
\frac{dP(t)}{dt} &= Q_i - Q(t), \\
Q(t) &= (1 + 4R(t))P(t), \\
\frac{dR(t)}{dt} + \lambda R(t) &= \alpha \lambda H(P - B(Q)).
\end{aligned}
\tag{17}
$$

Assuming that the process starts from rest, we have as initial conditions

$$
P(0) = R(0) = 0.
\tag{18}
$$

This system can be solved:

- numerically (see [7]):
  results show relaxation oscillations in $P(t)$ and $Q(t)$;

- analytically: see Section 6.

10

5 Comparison with slip model

Our discrete model presented in the preceding section, will now be compared with a, more or less analogous, discrete slip model derived by Den Doelder et.al., [7]. They used a model for slip at the capillary wall in agreement with a slip law first proposed by Greenberg and Demay, [2]. In this slip model, $v(1,t)$ can be either larger than zero or equal to zero, depending on whether slip occurs or not. When slip starts, the flow rate suddenly increases. The slip velocity at the wall is taken proportional to the maximum shear stress at the wall, which at its turn is proportional to the pressure $P(t)$. The appearance of slip is governed by an evolution equation of the same type as the one for $R(t)$. Thus,

$$v(1,t) = G(t)P(t),$$

where $G(t)$ satisfies (15) with $R(t)$ replaced by $G(t)$.
When slip occurs, the volumetric flow rate equals (instead of (7))

$$Q(t) = 2\int_0^1 rv(r,t)dr = v(1,t) + \int_0^1 r^2 w(r,t)dr.$$

In [7], the fluid is assumed Newtonian everywhere in the flow region, yielding

$$S(r,t) = w(r,t) = 4rP(t), \qquad \forall_{r \in [0,1]}.$$

Substitution of this relation for w into the equation for the flow rate leads to

$$Q(t) = (1 + G(t))P(t).$$

Hence, by comparing the latter relation with (14), we see that if

$$G(t) \rightarrow 4R(t),$$

exactly the same model follows.
Thus we conclude that in this approach, and in a mathematical sense, no difference between the two models based on either

- no-slip , spurt zone; or

- slip , no spurt zone;

exists.

6 Analytical calculations

The nonlinear system (17) can be solved analytically if we make use of asymptotics that are based on $\lambda \gg 1$ (fast transitions). For this, we distinguish four phases, of which phase 1. represents classical flow, phase 3. spurt flow, while the phases 2. and 4. are transition

phases from classical to spurt flow and vice versa, respectively. In the phases 1. and 3. the evolution equation (15) yields constant values for $R(t)$ (the very fast exponential evolution ($\propto \exp(-\lambda t)$, $\lambda \gg 1$) takes place in the transition phases). Hence, in phase 1., $R(t) = 0$, whereas in phase 3., $R(t) = \alpha$. During the very short ($O(\lambda^{-1})$) phases 2. and 4., $R(t)$ jumps from $0 \to \alpha$, and from $\alpha \to 0$, respectively. Since $R(t)$ is constant during the phases 1. and 3. (shape memory), the system (17) is linear then and can easily be solved. At the other hand, the transition phases are so short ($O(\lambda^{-1})$) that the changes in $P(t)$ according to (17) are also of ($O(\lambda^{-1})$) and, hence, negligible in an approximation for $\lambda \gg 1$. Thus, $P(t)$ may be taken constant during these phases, and again the system (17) is linear then and easy to solve.

Therefore, we distinguish the following four phases:

Phase 1. $\underline{0 < t < t_1}$; classical flow.

In this initial phase $P < B(Q)$ and, hence, $H(P - B(Q)) = 0$. Then $(17)^3$, with $R(0) = 0$, yields $R(t) = 0$. This reduces (17) and (18) to

$$
\begin{aligned}
\frac{dP}{dt} &= Q_i - Q(t), \qquad P(0) = 0, \\
Q(t) &= P(t),
\end{aligned} \tag{19}
$$

the solution of which reads

$$
P(t) = Q(t) = Q_i(1 - e^{-t}). \tag{20}
$$

The end of phase 1. is at $t = t_1$, where t_1 is the time where $P(t)$ reaches for the first time the switch curve $B(Q)$. Hence (see Figure 4), $P(t_1) = Q_1$, yielding

$$
t_1 = \ln\left(\frac{Q_i}{Q_i - Q_1}\right), \tag{21}
$$

provided $Q_i > Q_1$.
We note that $t_1 = O(1)$, which justifies our time scaling.

Phase 2. $\underline{t_1 < t < t_2}$: transition from classical to spurt flow.

Since $P(t)$ crosses $B(Q)$ from below at $t = t_1$, we assume that during this phase $P > B(Q)$, so $H(P - B(Q)) = 1$.
For this phase we introduce a new time scale: $\tau = \lambda(t - t_1)$, such that (17) becomes ($R = R(\tau)$, etc.)

$$
\begin{aligned}
\frac{dR}{d\tau} + R(\tau) &= \alpha, \qquad R(0) = 0, \\
\frac{dP}{d\tau} &= \frac{1}{\lambda}(Q_i - Q(\tau))(= O(\lambda^{-1})), \quad P(0) = Q_1, \\
Q(\tau) &= (1 + 4R(\tau))P(\tau).
\end{aligned} \tag{22}
$$

12

The solution of this system reads

$$
\begin{aligned}
P(\tau) &= P(0)(1 + O(\lambda^{-1})) \approx Q_1, \\
R(\tau) &= \alpha(1 - e^{-\tau}) \quad (\to \alpha), \\
Q(\tau) &= [1 + 4\alpha(1 - e^{-\tau})]Q_1 \quad (\to (1 + 4\alpha)Q_1).
\end{aligned}
\tag{23}
$$

We define the end of phase 2. as $\tau = \tau_2$, such that $e^{-\tau_2} = \lambda^{-1}$. This yields

$$
\tau_2 = \ln \lambda, \quad \text{or} \quad t_2 = t_1 + \frac{\ln \lambda}{\lambda} = t_1(1 + O(\lambda^{-1})).
\tag{24}
$$

So, indeed $\tau_2 = O(1)$, implying that the time that phase 2. lasts is very short $(O(\lambda^{-1}))$ compared to phase 1.

Phase 3. $\underline{t_2 < t \leq t_3}$; spurt flow.

In this phase we assume $P > B(Q)$ (see Figure 4), so $H(P - B(Q)) = 1$. Since $(23)^3$ yields $R(t_2) = \alpha(1 + O(\lambda^{-1})) \approx \alpha$, for $\lambda^{-1} \to 0$, $(17)^3$ renders $R(t) = \alpha$, for all $t \in (t_2, t_3)$. With the new time scale $\tau = (t - t_2)$, (17) reduces to $(P = P(\tau)$, etc.)

$$
\begin{aligned}
\frac{dP}{d\tau} &= Q_i - Q(\tau), \quad P(0) = Q_1, \\
Q(\tau) &= (1 + 4\alpha)P(\tau).
\end{aligned}
\tag{25}
$$

The solution of this system reads

$$
P(\tau) = \frac{Q(\tau)}{1 + 4\alpha} = \frac{Q_i}{1 + 4\alpha} + \left[Q_1 - \frac{Q_i}{1 + 4\alpha}\right] e^{-(1+4\alpha)\tau}.
\tag{26}
$$

Since phase 3. always runs along the line $P = Q/(1 + 4\alpha)$ in a $P - Q-$diagram, it must be so that if this line crosses the switch curve $B(Q)$ this happens in the point $P = B(Q_2) = Q_2/(1 + 4\alpha)$. According to (26), $Q(\tau) \to Q_i$, for $\tau \to \infty$. As $Q \to Q_i$, there are now two possibilities:

1. If $Q_i > Q_2$,

   then $P(\tau) \to Q_i/(1 + 4\alpha) > B(Q_i) = Q_2/(1 + 4\alpha)$
   In this case no transition takes place, and phase 3. tends to a final stationary spurt state, in which $(P(\tau), Q(\tau)) \to (Q_i/(1 + 4\alpha), Q_i))$, for $\tau \to \infty$.

2. If $Q_i < Q_2(< (1 + 4\alpha)Q_1$, see (16)) ,

   then a transition to classical flow takes place when $Q(t)$ reaches $Q_2 > Q_i$, and then phase 4. starts at $t = t_3(< \infty)$. Here, t_3 is such that $Q(t_3) = Q_2$, yielding

$$
t_3 = t_2 + \frac{1}{(1 + 4\alpha)} \ln \left(\frac{(1 + 4\alpha)Q_1 - Q_i}{Q_2 - Q_i}\right) .
\tag{27}
$$

13

We assume case 2. to hold, and we proceed with phase 4. We shall see that in this case relaxation oscillations occur.

Phase 4. $\underline{t_3 < t < t_4}$; transition from spurt to classical flow.

At $t = t_3$, $P(t)$ crosses the switch curve coming from above, so during this phase we assume $P < B(Q)$, and thus $H(P - B(Q)) = 0$

With the new time scale $\tau = \lambda(t - t_3)$, (17) reduces to ($R = R(\tau)$, etc.)

$$
\begin{aligned}
\frac{dR}{d\tau} + R(\tau) &= 0, \quad R(0) = \alpha, \\
\frac{dP}{d\tau} &= \frac{1}{\lambda}(Q_i - Q(\tau))(= O(\lambda^{-1})), \quad P(0) = Q_2/(1 + 4\alpha), \\
Q(\tau) &= (1 + 4R(\tau))P(\tau).
\end{aligned}
\tag{28}
$$

The solution of this system reads

$$
\begin{aligned}
P(\tau) &= \frac{Q_2}{(1 + 4\alpha)}(1 + O(\lambda^{-1})) , \\
R(\tau) &= \alpha e^{-\tau} \ (\to 0) , \\
Q(\tau) &= \frac{Q_2}{(1 + 4\alpha)}(1 + 4\alpha e^{-\tau}) .
\end{aligned}
\tag{29}
$$

Analogous to phase 2., phase 4. ends at $t = t_4 = t_3(1 + O(\lambda^{-1}))$.

At $t = t_4$, phase 1. starts anew, but now not from $P(0) = Q(0) = 0$, but from

$$
P = Q = Q_2/(1 + 4\alpha).
$$

This brings us to:

Phase 5. $\underline{t_4 < t < t_5}$; classical flow.

Analogous to Phase 1., the solution now reads

$$
P(t) = Q(t) = Q_i + \left(\frac{Q_2}{1 + 4\alpha} - Q_i \right) e^{-(t - t_4)}.
\tag{30}
$$

This phase ends at $t = t_5$ when $Q(t_5) = Q_1$, yielding

$$
t_5 = t_4 + \ln \left(\frac{Q_i - Q_2/(1 + 4\alpha)}{Q_i - Q_1} \right) ,
\tag{31}
$$

after which a phase identical to phase 2. follows.

Thus, a loop is followed as depicted by the dashed line in Figure 4. Since this dashed line is closed loop, it represents a periodic phenomenon. Its behaviour is of relaxation type,

14
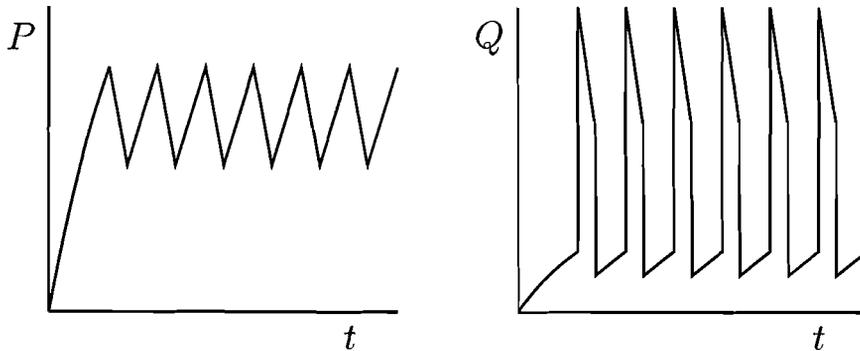
Figure 5: Relaxation oscillations for the pressure $P(t)$ and the volumetric flow rate $Q(t)$ ($Q_1 = 1, Q_2 = 3, Q_i = 2, \alpha = 1$, and $\lambda = 1000$)

because the phases 2. and 4. are extremely short. Therefore, we call this a relaxation oscillation. The period of one oscillation is $(t_3 - t_2) + (t_5 - t_4)$, or

$$T_{os} = \ln \frac{((1 + 4\alpha)Q_1 - Q_i)((1 + 4\alpha)Q_i - Q_2)}{(1 + 4\alpha)(Q_2 - Q_i)(Q_i - Q_1)} , \tag{32}$$

for $\lambda^{-1} \approx 0$. The behaviour of the pressure $P(t)$ and the volumetric flow rate $Q(t)$ during these relaxation oscillations is depicted in Figure 5.

Hence, the conclusion is that the obtained analytical results clearly predict relaxation oscillations. These relaxation oscillations occur if

$$Q_1 < Q_i < Q_2 < (1 + 4\alpha)Q_1 . \tag{33}$$

A relaxation loop consists of four distinct phases, of which in phase 1. the flow is classical, whereas in phase 3. spurt occurs; the phases 2. and 4. are relatively very short transition phases.

7 Results

Our model described by the system (17) is characterized by the parameter set $\{Q_1, Q_2, \alpha, \lambda\}$ plus the prescribed inlet flow rate Q_i. In the preceding section we have seen that dependent on the value of Q_i different types of capillary flow can occur. We distinguish three regimes for Q_i, knowing $Q_i < Q_1, Q_1 < Q_2 < Q_1$, and $Q_i > Q_2$. For the numerical results in this section, the following fixed values for the parameters are used:

$$Q_1 = 1 , Q_2 = 3 , \alpha = 1 , \lambda = 1000 .$$

15
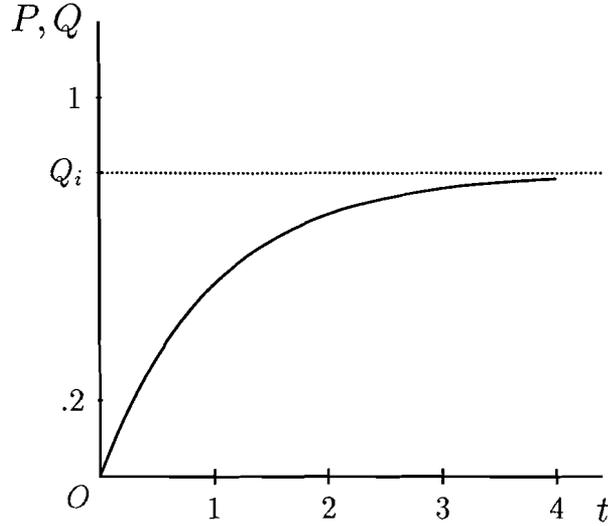
Figure 6: The pressure $P(t)$ and the flow rate $Q(t)$ as function of time t for $Q_i = 0.8 < Q_1$ (classical flow).

- In the first regime, $Q_i < Q_1$, the flow is classical, just like a Poiseuille flow. Since there is no spurt zone, the velocity profile is smooth. The pressure and the flow rate tend monotone to their stationary values, according to (20). This behaviour is depicted in Figure 6.

- In the second regime $Q_1 < Q_i < Q_2$, persistent relaxation oscillations occur. The flow periodically jumps from classical to spurt and vice versa, and large jumps in the pressure and, especially, the flow rate are found. The value of the flow rate is relatively high during spurt, and low during classical flow. Typical relaxation oscillations in $P(t)$ and $Q(t)$ in case $Q_i = 2$ are depicted in Figure 5.

- In the third regime $Q_i > Q_2$, the flow again tends to a stationary state, but now to one in which spurt occurs. The spurt zone is fixed to $R = \alpha$, and the pressure and flow reach the stationary values $\bar{P} = Q_i/(1 + 4\alpha)$, and $\bar{Q} = Q_i$, respectively, according to (26). In this regime we can further distinguish between $Q_i < (1 + 4\alpha)$ and $Q_i > (1 + 4\alpha)$. In case $Q_i < (1 + 4\alpha)$, an overshoot in both $P(t)$ and $Q(t)$ occurs, before they reach their final state. This overshoot at $t = t_1$ is depicted in Figure 7, for the case that $Q_i = 4$. If $Q_i > (1 + 4\alpha)$, no overshoot occurs; in this case the steady state is reached in a monotone way.

16
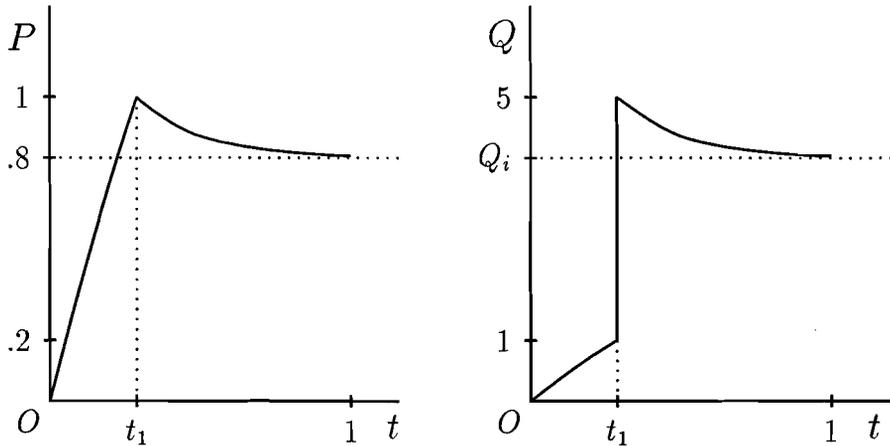
Figure 7: The pressure $P(t)$ and the flow rate $Q(t)$ as function of time t for $Q_i = 4 > Q_2$ (spurt flow).

8 Conclusions

In this case study, we have presented a discrete model for the capillary flow of a polymeric fluid, allowing for the occurrence of spurt flow. In spurt flow a very thin layer of very high shear rates exists near the wall of the capillary, while in the kernel the flow is almost uniform (like plug flow). Our model was built upon the assumption that the flow in both the kernel as well as in the spurt layer can be described by linear Newtonian fluid laws, however with quite distinct viscosities: the viscosity in the spurt layer is taken much smaller $(O(\varepsilon^{-1}), 0 < \varepsilon \ll 1)$ than the one in the kernel. At the wall of the capillary, a no-slip condition is maintained.
Our model is based on the fundamental concepts of:

- global mass balance for the compressible fluid in the barrel,

- equation of motion for the shear flow in the capillary,

- a global relation for the total flow rate through the capillary,

- a postulated evolution relation for the thickness of the spurt layer (inclusive a switch relation describing the forming or vanishing of a spurt layer).

We have shown that the model thus obtained was able to describe the distorted extrusion flow phenomenon called spurt. Spurt is manifested by relaxation oscillations in both the pressure in the barrel and the flow rate through the capillary or die of the extruder. The relaxation oscillations found here are of the type as depicted in Figure 5. Moreover,

17

Figure 8: The pressure $P(t)$ as function of time t for a loading process in which Q_i is stepwise increased at time steps T, with $T = 2.1$, according to the sequence $\{0.4, 0.8, 1.2, 1.8, 2.4, 3.6, 4.8\}$.

a finite range of prescribed inlet flow rates Q_i was found for which relaxation oscillations can occur. This was illustrated by the simulation of a realistic loading process, depicted in Figure 8, in which only for a restricted range of Q_i—values spurt oscillations show up. For Q_i—values below this range ($Q_i < Q_1$) the flow tends to a stationary classical (Poiseuille) flow, whereas for values beyond this range ($Q_i > Q_2$) the flow tends to a stationary spurt flow (having a fixed spurt layer).

We consider it important to notice here that the discrete model presented in Section 4 satisfies each of the four points listed in Section 3, which emanate from a three-dimensional theory (from [5]):

1. According to (33) spurt only occurs for a restricted range ($Q_i \in (Q_1, Q_2)$). The sudden increase in the flow rate Q at the time spurt starts, mentioned in Section 3, is clearly depicted in Figure 7.

2. For the range (Q_1, Q_2) mentioned in 1., relaxation oscillations are found as be seen from Figures 5 and 8.

3. The very fast transition from classical to spurt flow and v.v. is manifested by the high numerical value for λ in the evolution equation (15). In Section 6, it is shown that during the transition phases 2. and 4. the pressure remains constant, whereas the flow rate makes large jumps. The transition from classical to spurt flow takes place at a, normalized, pressure value $P = Q_1$, and that from spurt to classical flow at the *lower* value $P = Q_2/(1 + 4\alpha) < Q_1$.

18

4. During the spurt phase (i.e. phase 3. in Section 6) the normalized thickness of the spurt layer remains $R(t) = \alpha$, hence constant ('shape memory').

Hence, so far our discrete model is in accordance with the three-dimensional theory of [5].

In Section 5, we have shown that our discrete no-slip model renders exactly the same results as the discrete model of [7], which is based on a model with slip at the capillary wall (and without an internal spurt layer). Hence, in a mathematical sense, no diferences between these two models exist.

Relaxation oscillations in extrusion are many times observed in experiments, and they are often reported in literature. A lot of experimental data on especially extrusion instabilities can be found in the new book of Koopmans and Molenaar, [12]. Comparison of our analytical results as depicted in the Figures 5-8 with experimental results as they can be found in e.g. [7, Fig.9], [11, Fig.3] and [12] indicates a good *qualitative* agreement. However, for a *quantitative* agreement, some further modifications of the model presented here are needed. As shown in [11], for this at least a nonlinear evolution equation is needed. That this indeed can lead to an essentially improved quantitative agreement, is shown by Den Doelder et.al., [11], in which, amongst others, a nonlinear slip relation, relating the slip velocity to the square of the wall shear stress, is employed. Translated to our model, this would imply that relation (14) must become nonlinear (in that $P(t)$ must be replaced by $P^2(t)$). It remains a point for further research to investigate what are the consequences of this modification. Moreover, it once more stresses the fact that a theoretical basis for the (empirical) evolution equation for $R(t)$ is still missing. A further analysis of the results of the three-dimensional theory of the thesis of Aarts, [5] could possibly render some new insights in this aspect.

References

[1] J. Molenaar and R.J. Koopmans, Modeling polymer melt-flow instabilities, Journal of Rheology, **38** (1994), 99-109.

[2] J.M. Greenberg and Y. Demay, A simple model of the melt fracture instability, European Journal of Applied Mathematics, **5** (1994), 337-358.

[3] J.M. Piau and N.El. Kissi, Measurement and modelling of friction in polymeric melts during macroscopic slip at the wall, Journal of Non-Newtonian Fluid Mechanics, **54** (1994), 121-142.

[4] D.S. Malkus, J.A. Nohel and B.J. Plohr, Dynamics of shear flow of a non-Newtonian fluid, Journal of Computational Physics, **87** (1990), 464-487.

[5] A.C.T. Aarts, Analysis of the Flow Instabilities in the Extrusion of Polymeric Melts, Ph.D. Thesis, Eindhoven University of Technology (1997).

[6] A.C.T. Aarts and A.A.F. van de Ven, Instabilities in the extrusion of polymers due to spurt, Progress in Industrial Mathematics at ECMI94, H. Neunzert (Ed.), Wiley and Teubner, Chichester (1996), 216-223.

[7] C.F.J. den Doelder, R.J. Koopmans, J. Molenaar and A.A.F. van de Ven, Comparison of wall slip and constitutive instability spurt models, Journal of Non-Newtonian Fluid Mechanics, **75** (1998), 25-41.

[8] Kissi N.E., and Piau J.M., The different capillary flow regimes of entangled poly-dimethylsiloxane polymers: macroscopic slip at the wall, hysteresis and cork flow, Journal of Non-Newtonian Fluid Mech, **37** (1990), 55-94.

[9] A.C.T. Aarts and A.A.F. van de Ven, The occurrence of periodic distortions in the extrusion of polymeric melts. Submitted for publication in Continuum Mechanics and Thermodynamics.

[10] A.A.F. van de Ven, Comparing stick and slip models for spurt in the extrusion of polymeric melts. To appear in: Proceedings of ECMI 98.

[11] C.F.J. den Doelder, R.J. Koopmans and J. Molenaar, Quantitative modelling of HDPE spurt experiments using wall slip and generalised Newtonian flow. To appear in Journal of Non-Newtonian Fluid Mech, 1998.

[12] R.J. Koopmans and J. Molenaar, Polymer Melt Fracture, Marcel Dekker Inc., New York. To appear in 1999.